

Final paper: 'On the large angle anomalies of the microwave sky',
Copi Huterer, D. Schwartz and G. Starkman,
Mon.Not.Roy.Astron.Soc. 367 (2006).

Cora Dvorkin
June 2, 2006

Abstract

In this paper, the authors apply the multipole vector framework to full-sky maps from the first-year Wilkinson Microwave Anisotropy Probe (WMAP) data and show that the quadrupole ($l = 2$) and octopole ($l = 3$) are not statistically isotropic. They find that their planes are aligned and that, moreover, the plane that they define is perpendicular to the ecliptic plane. This fact is very unlikely. Even given the alignment of the quadrupole and octopole with each other, the alignment with the ecliptic is unlikely at > 98 per cent confidence level. Since the known Galactic foregrounds are located far from those of the observed sky, this suggests that the residual contamination of such foregrounds is unlikely to be the cause of the observed correlation. The cause for these special directions is still unknown. It could be due to non-standard inflationary physics, unexpected foregrounds, systematic artifacts in map making, deviations from General Relativity, or other unknown effects.

1 Introduction

The theory of inflation predicts a temperature anisotropy pattern that is statistically isotropic and gaussian random of zero mean. I will introduce now this two concepts.

A real scalar function $f(\theta, \phi)$ on a sphere can be expanded in multipole moments as

$$f(\theta, \phi) = \sum_{l=0}^{l=\infty} f_l(\theta, \phi)$$

$$f_l(\theta, \phi) = \sum_{m=-l}^{m=l} a_{lm} Y_{lm}(\theta, \phi) \quad (1)$$

For $f(\theta, \phi)$ to be a real function, a_{lm} needs to satisfy:

$$a_{lm}^* = (-1)^m a_{l-m} \quad (2)$$

Here, the term *gaussian random* means that the real and imaginary parts of a_{lm} are independent random variables that are distributed with a Gaussian distribution of zero mean. *Statistically isotropic* means that the variances of the a_{lm} depend only on l . Then,

$$\langle a_{l'm'}^* a_{lm} \rangle = C_l \delta_{ll'} \delta_{mm'}, \quad (3)$$

where C_l is given by

$$C_l \equiv \frac{1}{2l+1} \sum_{m=-l}^{m=l} |a_{lm}|^2, \quad (4)$$

and the set C_l with $l=0\dots\infty$ is called the angular power spectrum.

The distribution of gaussian variables is completely determined by their means and variances. Since the a_{lm} s have zero means, if the sky is indeed a realization of a gaussian random, statistically isotropic process, then all the information in a microwave background temperature map will be given by the angular power spectrum.

2 Multipole vectors

Multipole vectors provide an alternative representation of the complete set of information represented by the full-sky map [5]. They give information which is independent of the choice of the coordinate system. Because of this, multipole vectors are a better representation for looking for special directions in the sky.

In the multipole vector representation, $f_l(\theta, \phi)$ is written as

$$f_l(\theta, \phi) = A^{(l)} \left[\prod_{i=1}^l (\hat{v}^{(l,i)} \cdot \hat{\mathbf{e}}) - T_l \right], \quad (5)$$

where T_l is the sum of the possible traces of the first term $(\hat{v}^{(l,i)} \cdot \hat{v}^{(l,j)})$, $\hat{v}^{(l,i)}$ are unit vectors and $\hat{\mathbf{e}}$ is the unit vector in the (θ, ϕ) direction. In cartesian coordinates: $\hat{\mathbf{e}} = (\sin\theta\cos\phi, \sin\theta\sin\phi, \cos\theta)$.

An equivalent definition of the estimator C_l over the full sky is given by

$$C_l \equiv \frac{1}{2l+1} \int d\Omega [f_l(\theta, \phi)]^2 \quad (6)$$

So, plugging equation (5) into equation (6), we obtain

$$(2l+1)C_l = [A^{(l)}]^2 \int [\prod_j \hat{v}^{(l,i)} \cdot \hat{\mathbf{e}} - T_l]^2 d\Omega \quad (7)$$

For $l = 0$:

$$C_0 = 4\pi [A^{(0)}]^2 \quad (8)$$

For $l = 1$:

$$C_1 = \frac{4\pi}{3} [A^{(1)}]^2 \quad (9)$$

For $l = 2$:

$$C_2 = \frac{4\pi}{15} [A^{(2)}]^2 \left[1 + \frac{1}{3} (\hat{v}^{(2,1)} \cdot \hat{v}^{(2,2)})^2 \right] \quad (10)$$

We can observe from here that, due to the presence of the term $\hat{v}^{(2,1)} \cdot \hat{v}^{(2,2)}$, $A^{(2)}$ cannot be extracted solely from the angular power spectrum.

It is interesting to notice that this multipole vector expansion was first used by J. C. Maxwell in *A treatise of electricity and magnetism*, in 1891.

3 Relation to angular momentum dispersion

The alignment of the quadrupole and octopole was first pointed out by de Oliveira-Costa et al. in 2004 [4]. They denoted \hat{n}_l the axis that maximizes the angular momentum dispersion of each multipole when is chosen as the z-axis of the coordinate system:

$$(\Delta L)_l^2 \equiv \sum_{m=-l}^{m=l} m^2 |a_{lm}|^2 \quad (11)$$

They varied the direction of the z-axis over the sky and recomputed the $(\Delta L)_l^2$ for each choice. In this way, they were able to find the axis that maximizes the angular momentum dispersion. They had an interesting result: they found that $\hat{\mathbf{n}}_2 \cdot \hat{\mathbf{n}}_3 = 0.9838$. For $l = 2$ and $l = 3$ statistically independent, this alignment has only a 1.6 per cent chance of happening accidentally!

In the multipole vector framework, Copi et al. calculate the direction that maximizes the angular momentum dispersion. They obtain that $(\Delta L)_2^2$ is maximized in the direction normal to the plane defined by the two multipole vectors of the quadrupole:

$$\hat{\mathbf{n}}_2 = \pm \frac{\hat{\mathbf{v}}^{(2,1)} \times \hat{\mathbf{v}}^{(2,2)}}{|\hat{\mathbf{v}}^{(2,1)} \times \hat{\mathbf{v}}^{(2,2)}|}$$

I will explicitly show below their calculation of the axis $\hat{\mathbf{n}}_2$.

They write the angular momentum dispersion for $l = 2$ in terms of the angular momentum operator acting on the quadrupole function, as

$$(\Delta L)_2^2 = \int_{sky} |\hat{\mathbf{n}} \cdot \mathbf{L} Q|^2 d\hat{\mathbf{e}}, \quad (12)$$

and they maximize it over all possible unit vectors to find $\hat{\mathbf{n}}_2$.

The quadrupole function is:

$$Q(r) = (\hat{\mathbf{v}}^{(2,1)} \cdot \hat{\mathbf{e}})(\hat{\mathbf{v}}^{(2,2)} \cdot \hat{\mathbf{e}}) - \frac{1}{3} \hat{\mathbf{v}}^{(2,1)} \cdot \hat{\mathbf{v}}^{(2,2)}, \quad (13)$$

where $\hat{\mathbf{e}} = \frac{\mathbf{r}}{r}$. So, applying the angular momentum operator $\mathbf{L} = -ir\hat{\mathbf{e}} \times \nabla$ to the quadrupole function, we get

$$-i\mathbf{L}Q = (\hat{\mathbf{v}}^{(2,1)} \times \hat{\mathbf{e}})(\hat{\mathbf{v}}^{(2,2)} \cdot \hat{\mathbf{e}}) + (\hat{\mathbf{v}}^{(2,2)} \times \hat{\mathbf{e}})(\hat{\mathbf{v}}^{(2,1)} \cdot \hat{\mathbf{e}}) \quad (14)$$

Therefore, the quantity integrated can be written as

$$-i\hat{\mathbf{n}}\mathbf{L}Q = \hat{\mathbf{e}} \cdot [(\hat{\mathbf{v}}^{(2,1)} \times \hat{\mathbf{e}})(\hat{\mathbf{v}}^{(2,2)} \cdot \hat{\mathbf{e}}) + (\hat{\mathbf{v}}^{(2,2)} \times \hat{\mathbf{e}})(\hat{\mathbf{v}}^{(2,1)} \cdot \hat{\mathbf{e}})] \quad (15)$$

For an axis $\hat{\mathbf{n}} = (\sin\chi\cos\psi, \sin\chi\sin\psi, \cos\chi)$, and taking $\hat{\mathbf{v}}^{(2,1)}$ to be in the x-direction and $\hat{\mathbf{v}}^{(2,1)}$ and $\hat{\mathbf{v}}^{(2,2)}$ to define the x-y plane as $\hat{\mathbf{v}}^{(2,1)} \cdot \hat{\mathbf{v}}^{(2,2)} = \cos\omega$, the integral (12) can be made. The partial derivative of $(\Delta L)_2^2$ with respect to χ vanishes at $\chi = 0, \frac{\pi}{2}$ and π , where $\chi = 0$ and $\chi = \pi$ are maxima. Since ψ is not defined when $\sin\chi = 0$, the maximum angular dispersion is obtained in the direction normal to the plane defined by the two multipole vectors of the quadrupole: $\hat{\omega}^{(2;1,2)} = \pm \frac{\hat{\mathbf{v}}^{(2,1)} \times \hat{\mathbf{v}}^{(2,2)}}{|\hat{\mathbf{v}}^{(2,1)} \times \hat{\mathbf{v}}^{(2,2)}|}$.

In general, the *area vectors* will be defined as

$$\omega^{(l;i,j)} \equiv v^{(l,i)} \times v^{(l,j)} \quad (16)$$

Most of the statistics treated here will relate the dot-products of area vectors with one another and with physical directions of the sky.

The axis of maximum angular momentum dispersion for the octopole ($l = 3$) is calculated in the same way, where the octopole function is

$$\mathcal{O} = (\hat{\mathbf{v}}^{(3,1)} \cdot \hat{\mathbf{e}})(\hat{\mathbf{v}}^{(3,2)} \cdot \hat{\mathbf{e}})(\hat{\mathbf{v}}^{(3,3)} \cdot \hat{\mathbf{e}}) - T_3, \quad (17)$$

where

$$T_3 = \frac{1}{5} \hat{\mathbf{e}} \cdot [(\hat{\mathbf{v}}^{(3,1)} \cdot \hat{\mathbf{v}}^{(3,2)}) \hat{\mathbf{v}}^{(3,3)} + (\hat{\mathbf{v}}^{(3,2)} \cdot \hat{\mathbf{v}}^{(3,3)}) \hat{\mathbf{v}}^{(3,1)} + (\hat{\mathbf{v}}^{(3,3)} \cdot \hat{\mathbf{v}}^{(3,1)}) \hat{\mathbf{v}}^{(3,2)}] \quad (18)$$

In this case, it is difficult to find analytically the direction for which the angular momentum dispersion is maximized.

For the case where the three octopole vectors lie in the plane, the cross products of two are orthogonal to all three, and the maximum angular momentum dispersion axis (MAMD) is parallel to the area vectors of the three octopole planes. This approximation is a good approximation for the observed microwave background. For the cleaned full-sky map of Tegmark et al. (2003), (TOH):

$$|\omega^{(3;1,2)} + \omega^{(3;2,3)} + \omega^{(3;3,1)}| \simeq 0.8(|\omega^{(3;1,2)}| + |\omega^{(3;2,3)}| + |\omega^{(3;3,1)}|) \quad (19)$$

In the TOH map it can be seen that the three octopole area vectors surround the quadrupole area vector. Then, the MAMD, which is some average of the octopole area vectors, is close to the quadrupole axis; they are aligned.

4 Strange properties of the quadrupole and octopole

The microwave background seems to have several unusual properties on large scales. First, the power in the quadrupole is less than expected from the models that fit the rest of the angular power spectrum. The power in the octopole is also less than expected. By $l = 4$, the power is consistent with theoretical expectations. This was found by COBE and confirmed by WMAP [3]. It has also been seen by COBE and WMAP that the two-point angular correlation function

$$C(\theta) = \langle T(\hat{\mathbf{e}}_1) T(\hat{\mathbf{e}}_2) \rangle$$

is almost zero for angular scales between 60° and 170° (with $\hat{\mathbf{e}}_1 \cdot \hat{\mathbf{e}}_2 = \cos\theta$). This vanishing of $C(\theta)$ is due to the lack of quadrupole and octopole power. The authors of the paper believe that the observed lack of power at large angles justifies studying in detail the two most responsible multipoles.

4.1 The quadrupole

Figure 1 shows the $l = 2$ multipole from the Tegmark et al. (2003) map after subtraction of the kinetic quadrupole. The solid line is the ecliptic plane. The solid red diamonds are the multipole vectors (TOH map) and the open red diamond is the normal vector. The dotted line is the circle connecting the two multipole vectors for this map.

We can see that the circle connecting the two multipole vectors passes through the north ecliptic pole (NEP) and the south ecliptic pole (SEP). Then, the area vector $\hat{\omega}^{(2;1,2)}$ is on the ecliptic plane. $\hat{\omega}^{(2;1,2)}$ is also aligned with the equinoxes (EQX) and the dipole.

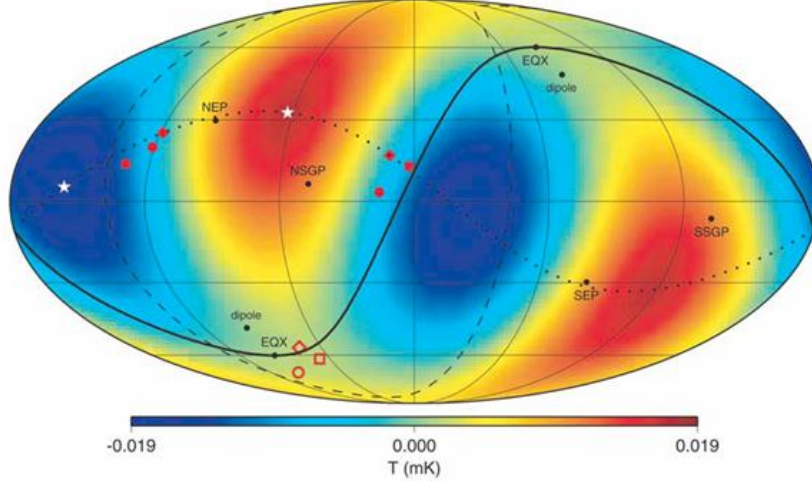


Figure 1: The $l = 2$ multipole from the Tegmark et al. (2003) cleaned map [1].

4.2 The octopole

Figure 2 shows the $l = 3$ multipole from the Tegmark et al. map. In this case, there are three multipole vectors (solid magenta diamonds for the TOH map) and three normal vectors (open symbols). The three dotted circles connect each pair of multipole vectors.

We can observe that the two great circles defined by $(\hat{\mathbf{v}}^{(3,1)}, \hat{\mathbf{v}}^{(3,2)})$ and $(\hat{\mathbf{v}}^{(3,1)}, \hat{\mathbf{v}}^{(3,3)})$ pass through the ecliptic poles. Therefore, $\hat{\omega}^{(3;1,2)}$ and $\hat{\omega}^{(3;1,3)}$ lie approximately on the ecliptic plane. The third area vector lies on the Supergalactic plane (but not on the ecliptic plane as the others do). So, the octopole is planar in a good approximation, even though is not exactly planar.

4.3 Relations between quadrupole and octopole

Figure 3 shows the $l = 2 + 3$ multipoles from the Tegmark et al. map. The solid line is the ecliptic plane, as before, and the dashed line represents the Supergalactic plane. The $l = 2$ multipole vectors are plotted as solid red diamonds, and the normal vector as an open red diamond. The $l = 3$ multipole vectors and area vectors are shown in magenta. The octopole axis is represented by the magenta star.

We can see from Figure 3 that the quadrupole normal vector $\hat{\omega}^{(2;1,2)}$ (the quadrupole axis $\hat{\mathbf{n}}_2$) is align with the octopole axis $\hat{\mathbf{n}}_3$ (magenta star). We can notice that the south of the ecliptic plane is

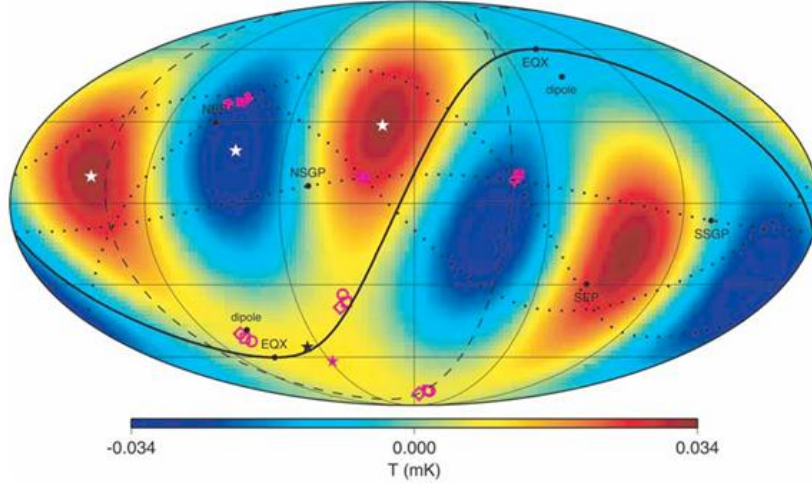


Figure 2: The $l = 3$ multipole from the Tegmark et al. cleaned map [1].

stronger in power than the northern part.

The alignment of the vectors with each other and with the Solar System is quantified by considering the dot-products A_i of the three octopole area vectors with the quadrupole area vector, and the dot-products D_i of the three octopole normalized area vectors with the quadrupole normalized area vector. The A_i and D_i were found unusually big (the maximum A_i was 0.851 and the minimum 0.762, while the maximum D_i was 0.953 and the minimum was 0.838).

It had been claimed before that the statistics applied to the area vectors A_i is not a robust statistic because A_i incorporates information of the lengths of the area vectors and, therefore, is not a good measure of alignment. In contrast, the authors claim that the A_i weight how well the multipole vectors define that plane: the more nearly orthogonal the vectors are, the better defined the plane is in the statistics. In the following section, I will summarize the statistics used by them.

5 Statistics

Two statistics were chosen to quantify the alignments: S and T statistics, which are defined as [2]

$$S \equiv \frac{1}{3}(A_1 + A_2 + A_3) \quad (20)$$

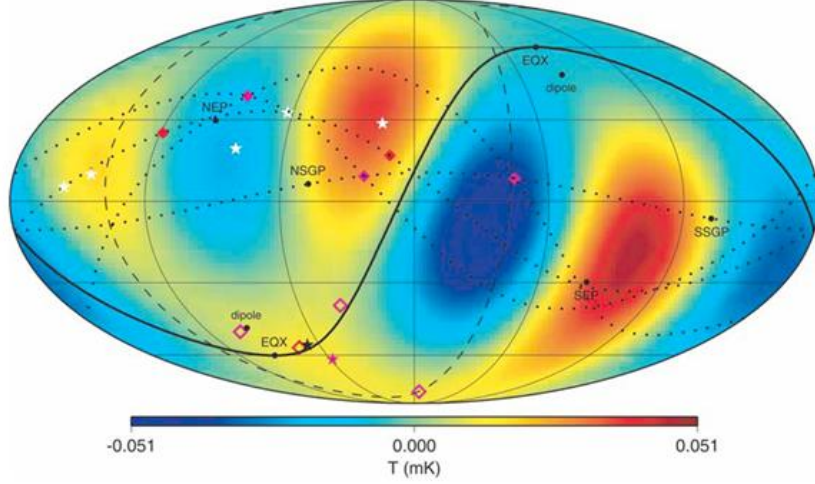


Figure 3: The $l = 2 + 3$ multipoles from the Tegmark et al. cleaned map [1].

and

$$T \equiv 1 - \frac{1}{3}[(1 - A_1)^2 + (1 - A_2)^2 + (1 - A_3)^2], \quad (21)$$

with $0 < A_i < 1$.

S and T can be viewed as distances to the vertex $(A_1, A_2, A_3) = (0, 0, 0)$. If the A_i are large (near 1), S and T will too.

If we are only interested in studying the alignment of some of the normals (and not all), we can generalize the statistics in the following way:

$$S^{(n,m)} = \frac{1}{m} \sum_{i=1}^{i=m} A_i \quad (22)$$

and

$$T^{(n,m)} = 1 - \frac{1}{m} \sum_{i=1}^{i=m} (1 - A_i)^2 \quad (23)$$

5.1 S and T statistics applied to quadrupole and octopole

In this paper, statistics applied to WMAP maps are compared to statistics applied to Monte Carlo simulations. The last ones were made with 100,000 realizations of Gaussian random, statistically isotropic maps with WMAPs pixel noise.

Figure 4 shows some of the histograms plotted in the paper.

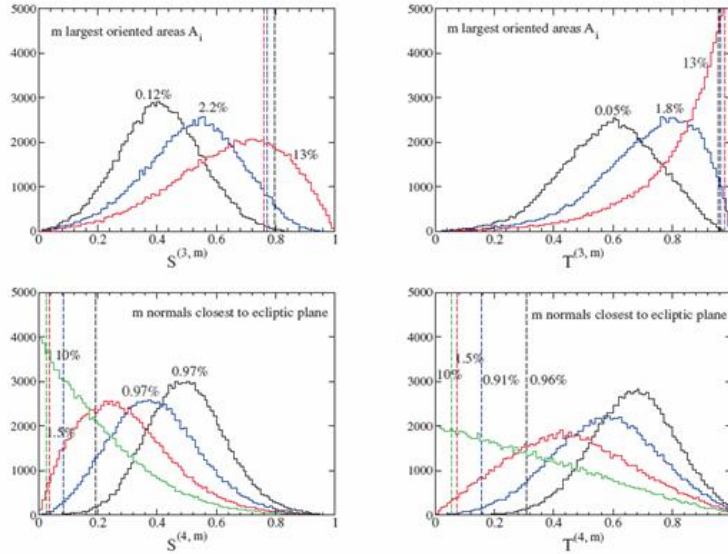


Figure 4: In the first row, dot-products of quadrupole and octopole area vectors, A_i are shown. In the second row, dot-products of area vectors with the ecliptic plane are plotted.

The numbers (%) in the plots show the number of Monte Carlo maps that have greater values than the one of WMAP (for example, a larger A_i) and the vertical lines correspond to specific values of WMAP for each m (for a TOH Doppler Quadrupole corrected map).

Statistics are stronger when all the vectors are considered ($m = n$), since in this case the probabilities are not dominated by one unusual alignment. When $m = 1$, both S and T statistics are, by definition, identical.

From Figure 4, we can conclude that the alignment between quadrupole and octopole, and between the normal vectors with the ecliptic plane are $> 98\%$ unlikely. Moreover, it was computed in this work that having taken the alignment of the quadrupole and octopole as given, there is a > 98 per cent confidence level alignment with the ecliptic plane, and the authors argue that this alignment is > 99.9 per cent unlikely. For the purpose of studying this, they took the correlation of the area vectors of the

quadrupole and octopole to be fixed. Then, they made 100,000 rotations for the TOH 's quadrupole and octopole and computed the $S(4,4)$ statistics for each direction in all of the rotated skies. The correlation with the ecliptic plane is greater than the one with the Supergalactic plane. This can be seen in Figure 3, too, where the four normals approximately surround the ecliptic.

It is worth mentioning that it has been suggested that one should study a large number of possible physical great circles to avoid an a posteriori focus on the ecliptic plane. The authors argue that there are precisely two great circles: the ecliptic and the Galactic one. The first one because WMAP orbits the Sun within the Solar System (and correlations could be due to local foregrounds), and the second one because of possible galaxy contamination. Correlations with the dipole direction are also worth studying because the Doppler dipole is a dominant foreground. The relevance of looking for correlations with the equinoxes and the Supergalactic plane is not so clear...

6 Multipole alignments for $l \leq 50$

It is also studied in this paper the alignment in higher multipoles (until $l = 50$). Copi et al. considered one multipole at a time and studied its planarity.

They computed 10^5 Monte Carlo realizations for $l < 2$ and 10^3 realizations for all other multipoles, and compared them with the S statistics applied to the TOH cleaned map. They ranked- order the S_{WMAP} among the S_{MC} , where the S statistics is now defined as

$$S \equiv \frac{1}{N_l} \sum_{i=1}^{N_l} |\omega_i \cdot \hat{\mathbf{n}}| \quad (24)$$

(with N_l the number of area vectors).

They found the $\hat{\mathbf{n}}$ that maximizes S and they rank-ordered. A low rank means that the multipole is planar (only a low percentage of the Monte Carlo maps is more planar), while a high rank indicates that the multipole is non-planar.

The motivation of this is to see if the low angular power spectrum observed at some multipoles is correlated in some way to the multipole vector alignments.

They tested the single multipole alignment of area vectors (for fixed l s). They found that for $l \geq 8$, the values of the S statistics differ substantially among the different maps considered (three full-sky maps: WMAP, ILC and LILC). Therefore, any claim based on this results would be weak.

7 Foregrounds

As it has been claimed before, contamination of maps should lead to a galactic and not to an ecliptic correlation. The authors show this with a quantitative analysis. They add the measured WMAP foreground to the full-sky maps and study how the directions defined by the octopole and quadrupole change.

They make the contaminated map in the following way:

$$T_{tot}(\hat{\mathbf{n}}) = T_{CMB}(\hat{\mathbf{n}}) + cT_{for}(\hat{\mathbf{n}})\sqrt{\frac{var(T_{CMB})}{var(T_{for})}}, \quad (25)$$

where c is the foreground fraction. It is reasonable to consider the contribution of residual foregrounds at large angular scales to be less than 10 per cent in power ($c \leq 0.3$). In the pure-foreground limit ($c = 1$), the normal vector of the quadrupole and the three normal vectors of the octopole move into the Galactic plane. It can be observed in Figure 2 that two of the octopole normals are about 10° of the Galactic poles. One could ask if this is due to residual Galactic contamination of the cleaned full-sky map. However, the alignment of the quadrupole and octopole area vectors with the North Galactic Pole is significant at < 90 per cent confidence level (compared to a 99 per cent confidence level correlation with the ecliptic plane).

So, the authors conclude that Galactic foregrounds lead to Galactic (neither ecliptic nor dipole) correlations of the quadrupole and octopole. Therefore, it is difficult to see how any foreground that has most of its power in the Galactic plane can lead to the Solar system correlations found in this paper.

8 Cut skies

Full-sky maps were studied in this paper. The authors claim that cuts in the sky introduce uncertainties in the reconstructed full-sky multipole vectors. They show how correlations vary when they introduce a sky cut. In general we cannot view the full sky because the Galaxy obscures our view, but there are ways to relate the cut sky decomposition a_{lm}^c to the true sky decomposition a_{lm}^t . The decompositions are related by

$$a_{lm}^c = \sum_{l'm'} W_{ll'mm'} a_{l'm'}^t, \quad (26)$$

where

$$W_{ll'mm'} \equiv \int_{S_{cut}} Y_{l'm'}^*(\Omega) Y_{lm}(\Omega) d\Omega \quad (27)$$

For longitudinal cuts (symmetric across the Galactic plane): $m = m'$. For each m , we have

$$a_l^c = \sum_{l'} W_{ll'} a_{l'}^t \quad (28)$$

W is not an invertible matrix because information was lost in the cut, but we can replace it by an invertible matrix \tilde{W} constructed from W removing the rows and columns with small eigenvalues. Then, an estimate value for the true decomposition is

$$\tilde{a}_l^t = \sum_{l'} \tilde{W}_{ll'}^{-1} a_{l'}^c \quad (29)$$

In this approximation, there is an error which comes from the fact that $\widetilde{W}^{-1}W \neq I$, because information was lost when the sky was cut. Therefore, the error can be written as

$$\begin{aligned}
& \langle |a^t - \widetilde{a}^t|^2 \rangle = \langle (a^t - \widetilde{a}^t)^* (a^t - \widetilde{a}^t)^T \rangle = \\
& = (I - \widetilde{W}^{-1}W) \langle (a_t)^* (a_t)^T \rangle (I - \widetilde{W}^{-1}W)^T = \\
& = (I - \widetilde{W}^{-1}W) C_l (I - \widetilde{W}^{-1}W)^T
\end{aligned} \tag{30}$$

They show that a cut in the sky introduces a significant uncertainty in the reconstructed multipole vectors and their normals, introducing uncertainties in the alignments tests. They plot the quadrupole and octopole probabilities for TOH maps, with different cuts of the sky. They show that the alignment become less unlikely as the cut is increased (less degrees), which is expected because if an event is unlikely, it becomes less unlikely in the presence of noise in the data. However, for relatively large cuts, the probabilities are consistent with their full sky values. In conclusion, the authors claim that a cut sky increases errors and shifts alignment values.

The alignments studied in this work are at large scales, so they can be seen in COBE maps (COBE has an angular resolution of 7°). Indeed, even though full-sky maps produced by COBE are very noisy, the alignments found with WMAP maps are consistent with COBE data.

9 Angular power spectrum: low - l anomalies.

It is worth noticing that there are also deviations from the predictions of the best Λ CDM model fit in the WMAP temperature angular power spectrum, which are at a comparable significance to the power deviation of the quadrupole (between 2.5 and 1.5 times the expected value). These deviations are found in $l \sim 20$, $l \sim 40$ and $l \sim 210$. Explanations given by Gordon and Hu (2004), Hannestad and Sloth (2005) and other references say that they could arise from fundamental physics. There are other anomalies in the low-multipole sky, some of them are: $l = 6$ is very planar and is closely aligned with the ecliptic, there is a deficit in the ecliptic planar power compared to the ecliptic polar power, etc.

10 Conclusions

The multipole vectors provide a complete representation of a scalar function on a sphere, and they are a good way to study alignments and correlations in the microwave sky. Octopole and quadrupole have unexpected properties individually and together. The S and T statistics were used to study correlations; they were applied to the area vectors of the quadrupole and octopole. The alignment of the quadrupole and octpole planes was confirmed at 99 per cent confidence level, and their planes were found to be aligned with the motion of the Solar system. In particular, they are perpendicular to the ecliptic plane at ~ 98 per cent confidence level. They are also perpendicular to the Galactic poles at > 99 per cent confidence level. They studied the case where the alignment of the quadrupole and octopole planes is given and, in this case, the alignment with the ecliptic plane remains at 99 per cent confidence level. The correlations with the equinoxes and dipole remain, but the correlation with the

Galactic poles does not persist. This supports the reality of the alignment with the ecliptic plane, and suggests that the alignment with the Galactic poles is accidental. It can be seen in Figure 3 that the ecliptic plane separates the weaker power of the northern ecliptic sky from the stronger power of the southern ecliptic sky. This information is not contained in the statistics done with the area vectors. In this work, full-sky maps from the first-year WMAP data were used.

With the purpose of studying if Galactic foregrounds were biasing the results, they explored the properties of the multipole vectors in maps with foregrounds. They also studied maps with cuts. They have shown that it is necessary to add large foreground contaminations in order to make the full-sky map multipole vectors look like those from the foreground maps. The multipole vectors of the full-sky were found to be in different locations to those from the foreground maps.

They studied the effect of making cuts in the sky. They claim that even small cuts lead to large uncertainties in the results. They checked that the results are consistent with the correlations obtained from COBE data.

Finally, one can think about the deep causes that explain the results found in this paper. They could be explained either by an ecliptic correlated foreground or by new physics. On the experimental side, there is a new independent coming probe: measurements of temperature and polarization by the Planck experiment. Perhaps a new inflationary model, or a deviation from General Relativity will need to be considered.

References

- [1] C. Copi, D. Huterer, D. Schwartz and G. Starkman, *Mon.Not.Roy.Astron.Soc.* 367 (2006).
- [2] D. J. Schwarz, G. D. Starkman, D. Huterer, C. J. Copi, *Phys. Rev. Lett.*, 93, 221301 (2004)
- [3] Wilkinson Microwave Anisotropy Probe (WMAP) Three Year Results: Implications for Cosmology, Spergel et al., *astro-ph / 0603449v1* (2006).
- [4] A. de Oliveira-Costa, M. Tegmark, M. Zaldarriaga and A. Hamilton, *Phys. Rev. D* 69, 063516 (2004).
- [5] C. Copi, D. Huterer and G. Starkman, *Phys. Rev D.* 70, 043515 (2004).